Atomic Force Microscopy Images of Ion-implanted 6FDA-pMDA Polyimide Films

XINGLONG XU, M. R. COLEMAN

Department of Chemical Engineering, University of Arkansas, Fayetteville, Arkansas

Received 12 August 1996; accepted 26 February 1997

ABSTRACT: The surface structure and morphology of ion-beam irradiated 6FDA-pMDA films were investigated using atomic force microscopy (AFM). A beam of 140 keV N^+ ions with a low current density was used in this work. Three irradiation fluences ($2 \times 10^{14}/cm^2$, $1 \times 10^{15}/cm^2$, and $5 \times 10^{15}/cm^2$) were chosen to represent three different regimes of ion-beam influence on material properties based upon previous diffusion and gas permeation results of implanted polyimide films. Detailed roughness and bearing analyses of the AFM images indicate that freestanding polyimide films have deep surface valleys which can extend to a depth of several micrometers. Ion-beam irradiation, even at a small dose, alters the microstructure of the surface layer and forms a modified layer which eliminates the initial deep valleys. The AFM analysis shows that small fluence irradiation induced microvoids in the surface layer of the polymer, and high fluence irradiation resulted in a large number of small-size microvoids in the surface. All of these results agree well with the ion-beam irradiation effects on iodine diffusion and gas permeation properties of the polyimides. A ripple topographical structure with a wavelength of 25 μm and an amplitude of 2 nm was also observed for irradiated samples. © 1997 John Wiley & Sons, Inc. J Appl Polym Sci **66:** 459–469, 1997

Key words: polyimide; ion beam irradiation; gas separation membrane; atomic force microscopy; morphology

INTRODUCTION

Over the past few decades, polyimides have attracted considerable attention for application in fields ranging from microelectronics to gas separation membranes.[1–10] Polyimides are widely used because of their excellent physical and mechanical properties, including good thermal stability, excellent mechanical properties, low dielectric constant, and good dimensional stability. These polymers are used extensively in microelectronics in interconnection and packaging applications such as passivation layers and interlayer dielectrics in high-density thin-film interconnections in multichip modules.[1–4] Numerous attempts have also been made to use polyimides as nonlinear-optical materials.[5,6] Recently, 6FDA-based polyimides were found to have very good gas transport properties which make them attractive for use as permselective layers in gas separation membranes.[7–10]

Ion implantation has been successfully used in microelectronics[11,12] and has become a routine process in the production of microelectronic devices. Ion-beam technology is also used in diverse material processing systems because it can significantly modify the properties of a material in an easily controlled fashion. Changes in electrical and optical properties, as well as chemical structure of polyimides induced by ion implantation, have been investigated by several groups.[13–16] Recently reported work indicates that ion-beam irradiation can also greatly modify the transport

Correspondence to: M. R. Coleman.

Contract grant sponsor: Presidential Faculty Fellows Program, National Science Foundation; contract grant number: CTS-9553267.

Journal of Applied Polymer Science, Vol. 66, 459–469 (1997)
 CCC 0021-8995/97/030459-11

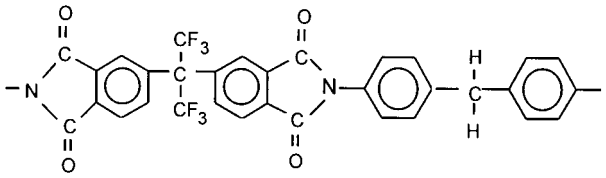

Figure 1 The structure of 6FDA-pMDA polyimide used in the work.

properties of small molecules within a polymer matrix.[16–18] Ion implantation was shown to have a significant effect on iodine diffusion and gas permeation behavior within polyimide films modified by ion bombardment. Xu and colleagues[16,17] reported that ion-beam irradiation with low fluence causes enrichment of iodine atoms in the surface modified layer but prevents further diffusion beyond that modified layer, and also that in case of high fluence irradiation no iodine can diffuse into the film. Xu and associates[17,18] also reported that ion irradiation at low fluence led to a large increase in both H_2 and CH_4 permeabilities with a decrease in H_2/CH_4 selectivity, whereas ion bombardment at high fluence resulted in a large increase in H_2 permeability with a corresponding increase in H_2/CH_4 selectivity. These large changes in properties induced by ion-beam bombardment imply that ion-beam irradiation can alter the structure of the surface layer of polymers. However, microstructural changes of the surface layer, such as topographical and morphological modification resulting from ion-beam bombardment, remain unclear and further investigation is necessary.

Atomic force microscopy (AFM) provides an ideal method of observing the surface structure of insulating and conducting materials at micron (a few nanometers spatial resolution for scanning up to 113 μm) and molecular levels (for small scanning range).[19–23] Unlike classic microscopic techniques, AFM allows the acquisition of 3-D topographic data with a high vertical resolution (down to 0.05 nm) in selected areas with lateral sizes at nanometric scale. Accurate and quantitative data about surface morphology are provided over a wide range of magnifications and can be interpreted by accounting for artifacts which may be introduced by the finite size of the AFM tip. In recent years, AFM has been used extensively to investigate the surface structure and morphology of membranes, including integrally skinned phase-

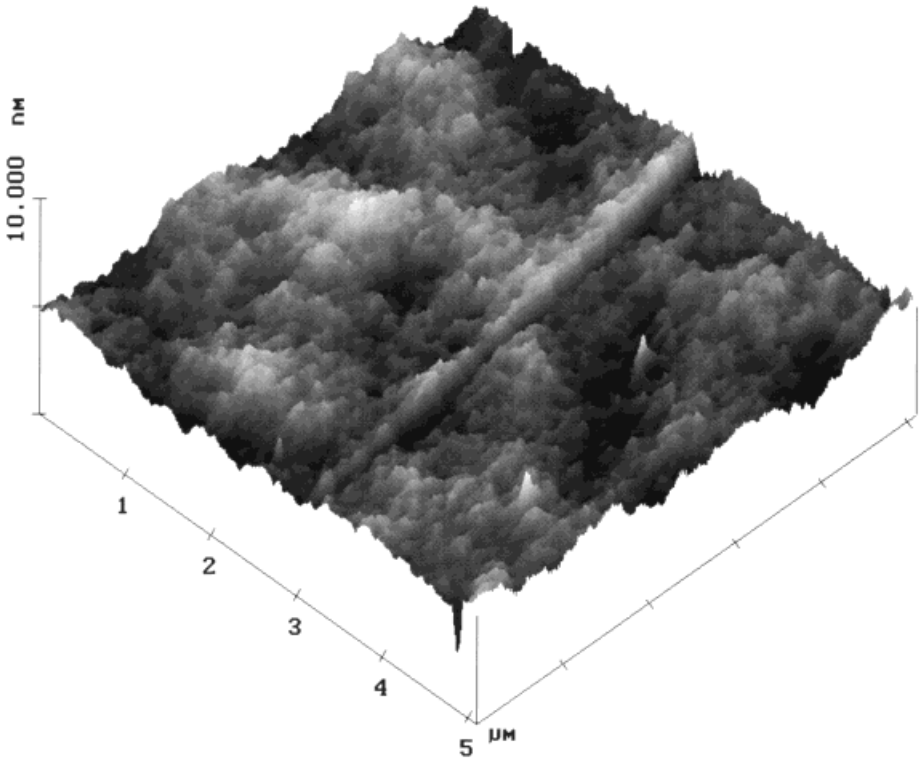

Figure 2 A typical surface-plot AFM image of the 6FDA-pMDA polyimide film. The area of the image is 5 × 5 μm in x, y-plane. The range of the vertical axis (z-axis) is 5 nm.

inversion membranes. Fritzsche and coworkers[24–26] determined membrane pore sizes by measuring the horizontal distance of a surface valley in the section analysis of AFM images. This method is based on the results of AFM analysis of the surface structure and morphology of a series of polymeric membranes.[24–26] However, this method can only measure the micropore size and micropore size distribution along a straight line in an AFM image. It cannot be used to give global information about the micropore size and size distribution over a surface area. Therefore, a complementary method will be used to analyze the entire surface area. This article presents preliminary results of ion-beam irradiation-induced topographical changes in a 6FDA-based polyimide using AFM, and discusses the evolution of physical structure of polyimide films modified by ion-beam bombardment using AFM.

EXPERIMENTAL

Materials

The structure of the polyimide (6FDA-pMDA) used in this study is shown in Figure 1. The 6FDA-pMDA was synthesized via the general reaction of a dianhydride (6FDA) with a diamine (pMDA), with final imidization effected by chemical methods.[27] The monomers and the solvents were purchased from Aldrich Chemical and Hoechst-Celanese Corporation. The monomers were purified using recrystallization or sublimation. For the 6FDA-pMDA synthesis, equimolar quantities of pMDA and 6FDA were charged with dimethyl acetimide to a flask under an argon atmosphere. Following dissolution of the monomers, the reaction mixture was heated to 25°C for approximately 24 h to form poly(amic acid). The poly(amic acid) solution was then cooled to 20°C, and a solution of trimethylamine and acetic anhydride was added to the mixture to promote chemical imidization. Following heating at 25°C for 24 h, the polymer solution was poured into an excess of ethanol to precipitate the polyimide.

The 6FDA-pMDA polyimide films used in this work were thick, dense films (25–50 μm) which were solution-cast from methylene chloride using standard techniques. Samples of the 6FDA-pMDA were dissolved in methylene chloride to form a solution which was between 5 and 10% polymer by weight. The 25–50-μm-thick films were cast from a filtered solution into a glass dish

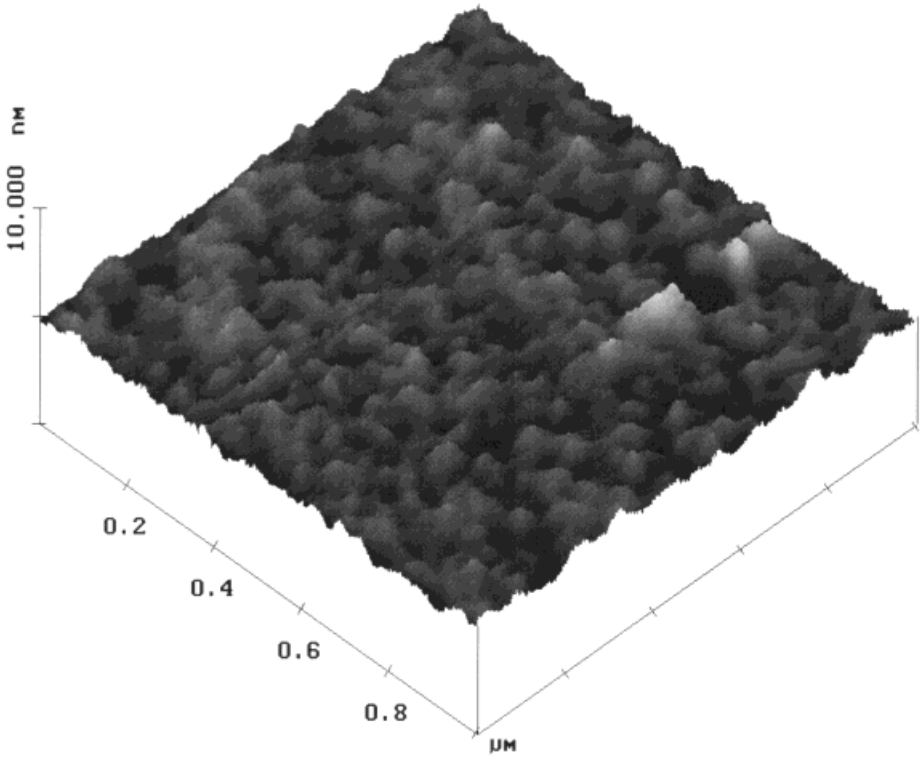

Figure 3 Enlarged surface-plot AFM image of the same sample as in Figure 2. Image area is 1 × 1 μm in x, y-plane and the range of z-axis is 5 nm.

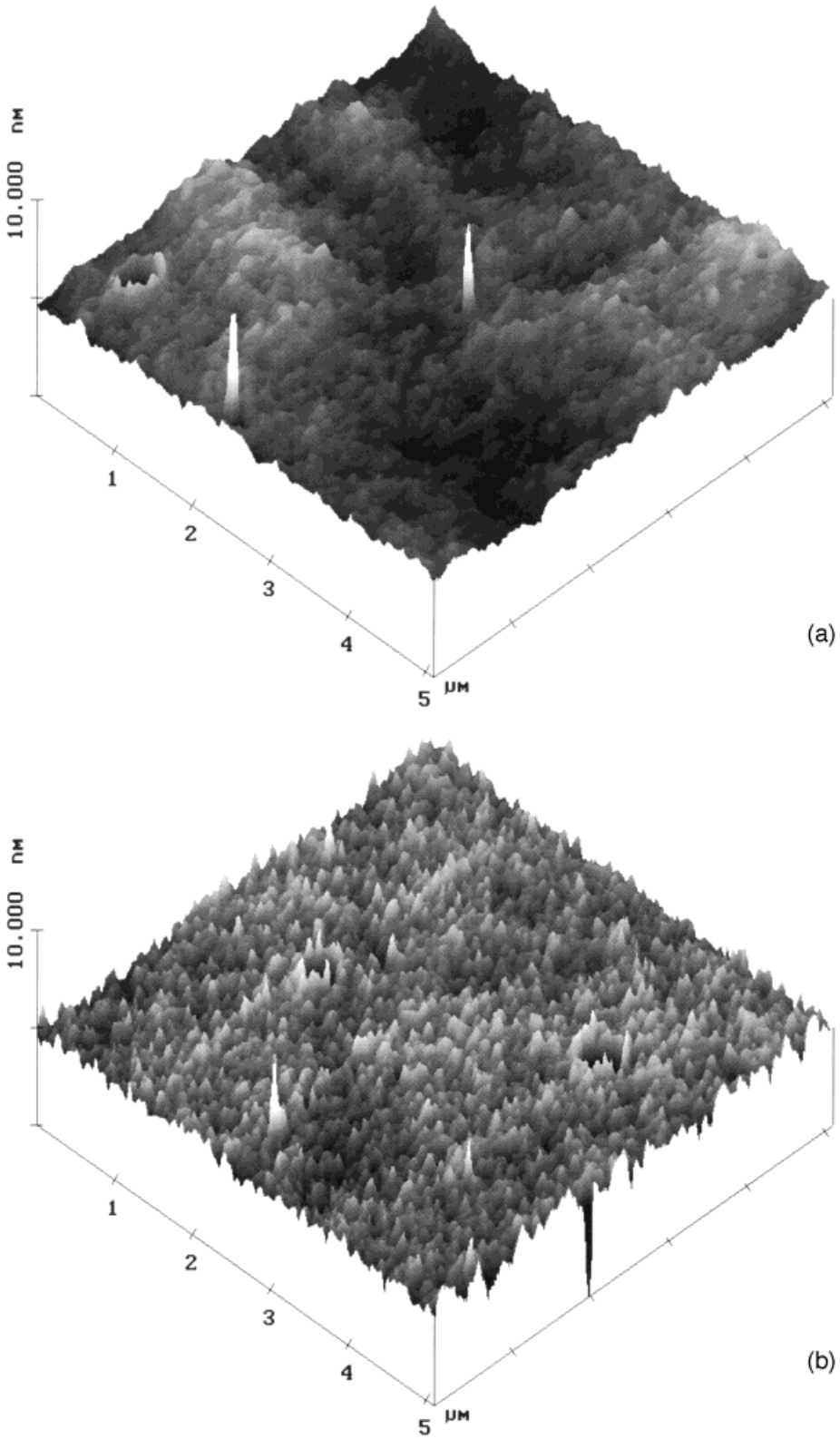

Figure 4 Surface-plot AFM images of ion beam-irradiated 6FDA-pMDA polyimide films. Image area is 5 × 5 μm in the x, y-plane and the range of z-axis is 5 nm. Irradiation fluence: (a) 2×10^{14} N^+/cm^2; (b) 1×10^{15} N^+/cm^2; (c) 5×10^{15} N^+/cm^2.

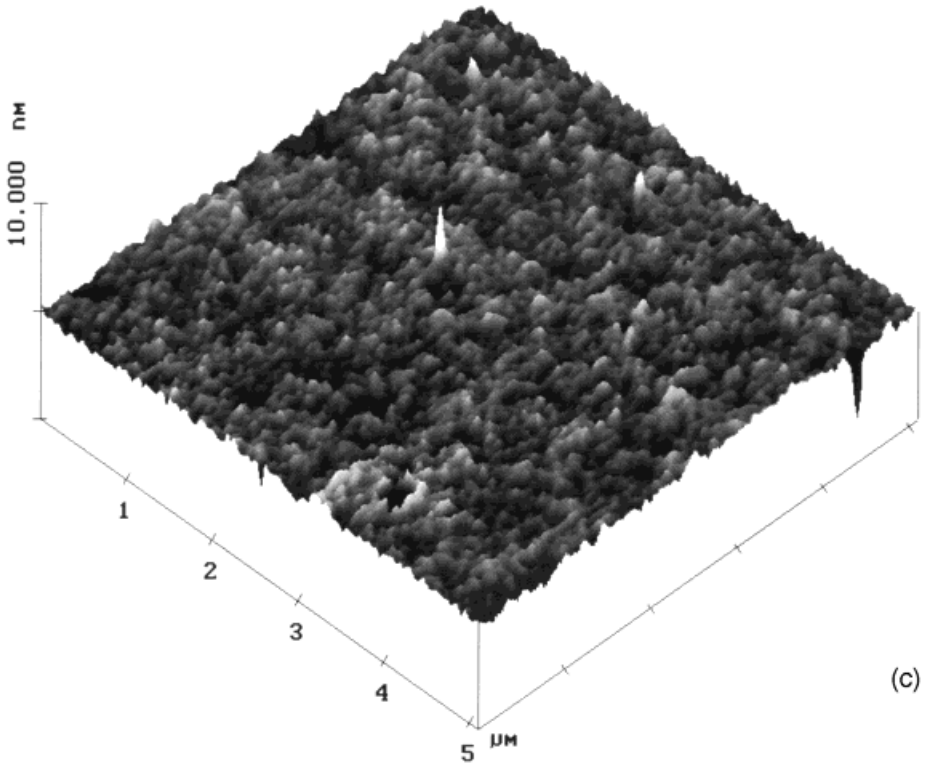

Figure 4 (*Continued from the previous page*)

in a glove bag. The films were cast in a glove bag to regulate the rate of solvent evaporation. After drying, the dishes were submerged in water to assist in the removal of the film from the glass. The films were further dried in air at room temperature for 12 h. Finally, the dense films were dried under vacuum at temperatures up to 250°C for several days to remove residual solvent.

Ion Implantation

Ion implantation was performed using a semiconductor ion implantor IM 200 at the Ion Beam Laboratory, Shanghai Institute of Metallurgy, Chinese Academy of Sciences. All of the implantations were done using 140 keV N^+ ions at room temperature. The beam-current densities used in this work were maintained at low levels (≤ 1 μA/cm^2) to avoid heating of the samples. The incident beam was perpendicular to the surface of the samples. The implantation fluence ranged from 2×10^{14} to 5×10^{15} N^+/cm^2. The thickness of the ion-beam modified layer was determined to be approximately 490 nm using ($R_p + \Delta R_p$) by TRIM '94 code.[28]

AFM Measurement

The atomic force microscope used in this study was a Digital Instruments NanoScope® III at the High Density Electronic Center at the University of Arkansas (Fayetteville, AR). All the measurements were performed in air using a contact mode. The AFM is equipped with a software system which allows a variety of analyses of AFM data,[29] including section analysis, bearing analysis, and roughness analysis.

The AFM software's bearing analysis system provides a method of plotting and analyzing the distribution of surface height of a sample and determines the percentage of the surface that lies above or below a given height. The area mode allows the data for a given area to be used in the calculation of the bearing and histogram curves. The area mode was used in the AFM analysis of the ion-beam irradiated samples as well as the reference sample, with an analysis area of almost the entire range of the sample (5×5 μm). The highest peak height was taken as depth reference.

The AFM software's roughness analysis system allows the calculation of several roughness parameters for the entire image or within an area specified by the user. The peak calculation, which gives information about peak count and average peak height, was used. Calculations were based on a threshold height defined by the user. There are two types of thresholds: (1) absolute value, or (2) relative value in a unit of the standard devia-

tion of the z value (%). Zero z value was chosen as the reference for the absolute value height threshold in the peak calculation. The peak count is the number of surface peaks taller than the threshold. If the AFM image is inverted, results from the peak calculation in the roughness analysis give corresponding information about surface valleys of the noninverted image.[29] The mean roughness was calculated using the following formula:

$$R_a = \frac{1}{L_x L_y} \int_0^{L_y} \int_0^{L_x} |f(x, y)|\, dx\, dy$$

where $f(x, y)$ is the surface relative to the center plane, which is a flat horizontal plane separating the surface into two equal volumes, and L_x and L_y are the dimensions of the surface. Roughness analysis was performed over a 5- $\times$ 5-μm area of the samples with an absolute value height threshold for both inverted and noninverted images.

RESULTS AND DISCUSSIONS

The polyimide films were bombarded at ion fluences in the following ranges: (1) small fluence at 2×10^{14} N^+/cm^2, (2) intermediate fluence at 1×10^{15} N^+/cm^2, and (3) high fluence at 5×10^{15} N^+/cm^2. As mentioned previously, these ranges were defined based on the results of ion-beam irradiation effects on diffusion and gas permeation properties of polyimide films.[16–18] The base 6FDA-pMDA film was transparent with a light yellow color. The color of the film changed with the implantation fluence from yellow to brown to black with a metallic luster as the irradiation dose was increased from 2×10^{14} N^+/cm^2 to 5×10^{15} N^+/cm^2. A typical surface-plot AFM image of a reference 6FDA-pMDA film is shown in Figure 2. The area of the image is 5 $\times$ 5 μm in the x, y-plane with an expanded z-axis of 5 nm. A two-level structure, which is composed of bold chains that, in turn, consist of nodulelike structure, can be observed.[24–26] A 5-fold enlarged AFM image of the base polyimide is given in Figure 3. The nodulelike structure can be seen more clearly in the expanded image. Figures 4(a)–(c) show the surface-plot AFM images of the three ion-irradiated 6FDA-pMDA samples. These figures use the same x, y-plane dimension and z-axis expansion as those in Figure 2 to facilitate comparison between the images. Slight differences can be perceived between the images of the nonimplanted sample

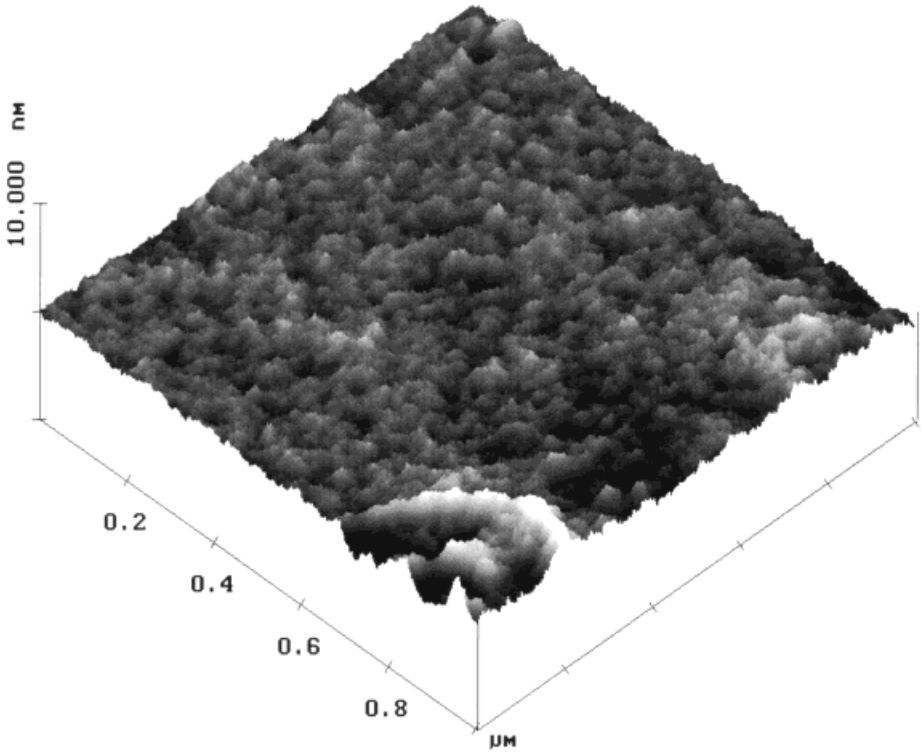

Figure 5 Enlarged surface-plot AFM image of the same sample as in Figure 4(c). Image area is 1 $\times$ 1 μm in x, y-plane and the range of z-axis is 5 nm.

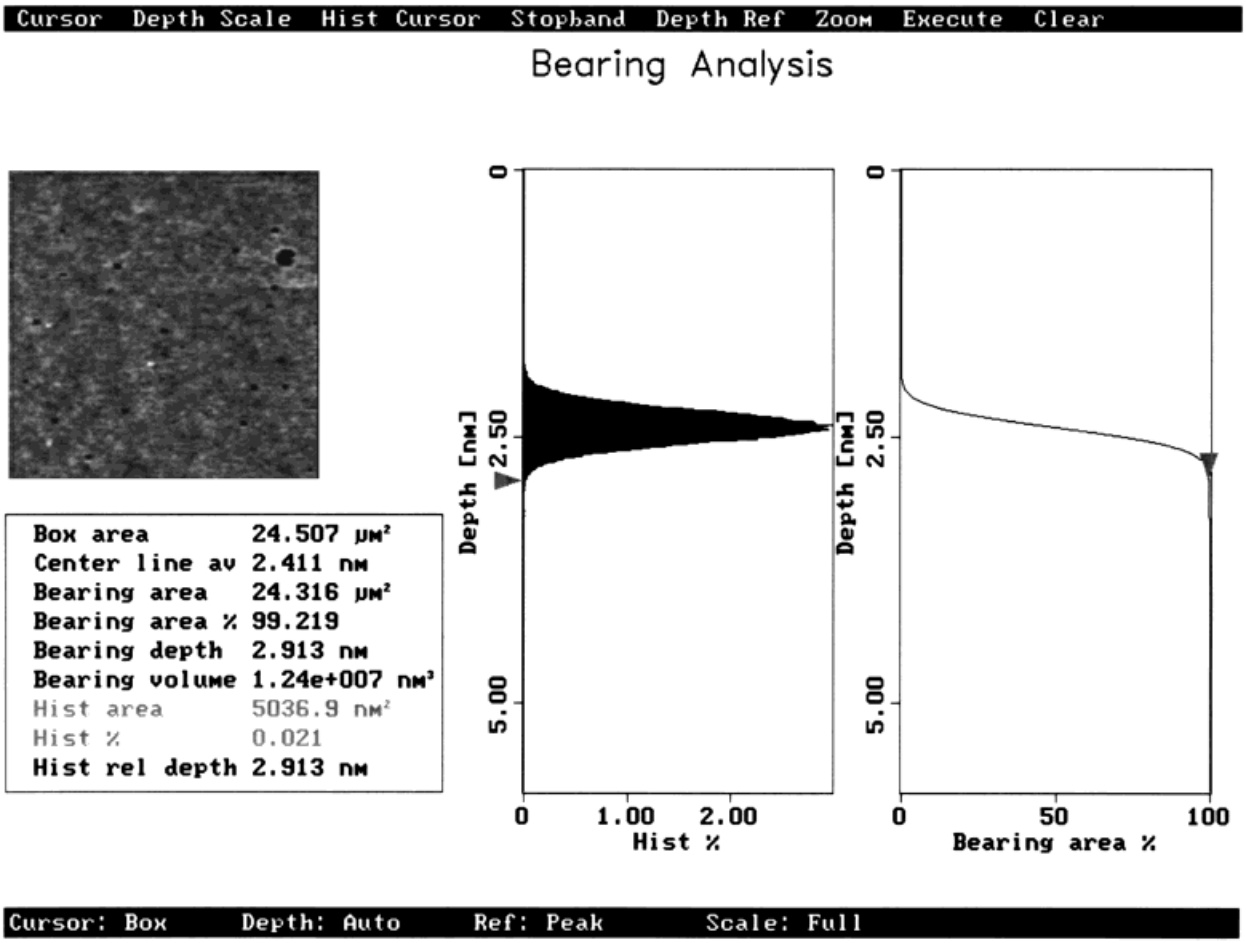

Figure 6 A typical bearing analysis plot of the 6FDA-pMDA sample implanted with $5 \times 10^{15}/\text{cm}^2$.

and the sample implanted at 2×10^{14} N^+/cm^2. The two-level structure persisted following the small-fluence irradiation. The AFM image of the sample irradiated with 1×10^{15} N^+/cm^2 shows a different topography. The two-level structure has disappeared, with the bold chains no longer present. Meanwhile, the surface consists of small, cone-like structures of smaller dimension than the nodule-like structure of the reference polymer. At an irradiation fluence of 5×10^{15} N^+/cm^2, the surface of the sample was very flat and a small, nodulelike structure appeared instead of the small cones observed at the intermediate dose. The small, nodulelike structure can be seen more easily in the enlarged AFM image (Fig. 5) of the highest-fluence implanted sample. A large, shallow hollow located at the corner of this image is also seen.

Although the descriptions of Figures 2–5 clearly illustrate the topographical evolution of the polyimide 6FDA-pMDA film at different stages of ion-beam irradiation, they are descriptive and qualitative. In order to obtain quantitative information, bearing and roughness analyses of the AFM samples were performed. Figure 6 is a typical bearing analysis plot of a sample which was implanted with 5×10^{15} N^+/cm^2. All of the 6FDA-pMDA samples exhibited similar profiles shapes for the surface height distribution (Gaussian distribution) but the distributions were shifted to different depths. In order to compare the effect induced by ion-beam irradiation, the distributions were normalized by neglecting those contributions which were so small that they were not visible on the bearing plot. This normalization process influenced the position but not the shape of the distribution. A comparison of the surface height distributions of the 6FDA-pMDA films is given in Figure 7. The surface height distribution of the nonimplanted sample extended up to 3 nm in depth. This depth range decreased with increasing ion-beam irradiation fluence. At a flu-

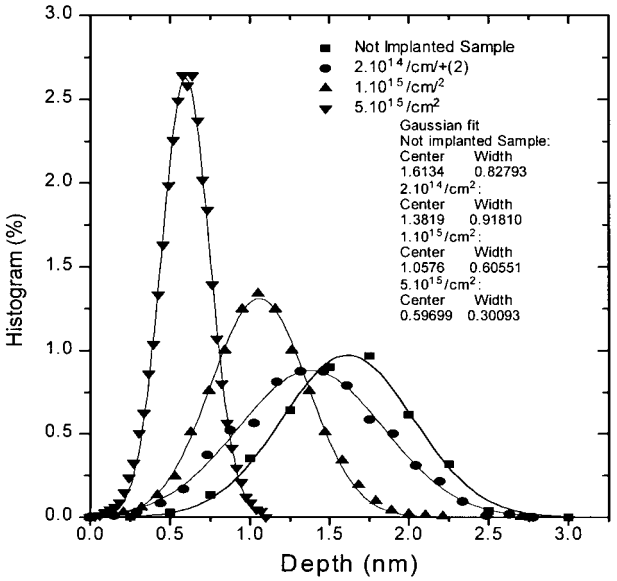

Figure 7 Comparison of the bearing analysis between the non-implanted sample and samples implanted at different fluences. These distributions have Guassian distribution characteristics. The fit parameters of Guassian distribution are also listed in the figure.

ence of 5×10^{15} N^+/cm^2, a sharp distribution can be observed within a depth range of only 1.1 nm. This value is only 36% of the value for the non-implanted sample. The results of a fit of the depth profile to a Gaussian curve are given in Figure 7. The distribution width is larger for the small-fluence irradiation sample than for the base material, whereas the distribution width decreases with increasing fluence for the intermediate and high fluences. This implies that for small fluence, ion irradiation induced a broader surface height distribution than that of the non-implanted sample, whereas intermediate- and high-fluence ion bombardment gives rise to narrower distributions.

The results of the roughness analysis are given in Tables I and II, and in Figure 8. The mean roughness decreased with increasing ion irradiation fluence (see Table I), which is consistent with the bearing analysis shown in Figure 7. With a fixed absolute value (0.4 nm) as the threshold value, the peak count increased with the implantation dose, reached a maximum (706), then dropped to a low value of 107 for the highest implantation fluence. Table II gives the same results in terms of peak count in different height intervals. The evolution of the peak number and peak height induced by ion-beam irradiation can clearly be seen from Table II. Though there are a small number of peaks whose heights are below 0.5 nm, the majority of the peaks are higher than 0.5 nm for the nonimplanted 6FDA-pMDA sample. The small-dose implantation at $2 \times 10^{14}/cm^2$ results in a large increase in the peak number. The high-fluence irradiation at $5 \times 10^{15}/cm^2$ induced a very large number of small peaks in the 0.2–0.4 nm height interval and a significant reduction of the peak number in the $>$ 0.5 nm height range.

The surface valley analysis results are summarized in Figure 8, in which the valley numbers are plotted as a function of their depth. The nonimplanted sample has very deep valleys with depths extending well beyond 0.4 μm to a maximum depth of 8.5 μm. Ion irradiation dramatically modifies the valley depth distribution. For all of the implanted samples, the valley depths extend to just a few nanometers and the maximum valley numbers increase sharply with the ion-implantation fluence. Small-dose irradiation at 2×10^{14} N^+/cm^2 produces a large increase in the valley number. High-fluence irradiation at 5×10^{15} N^+/cm^2 generates a large number of small valleys in the 0.2–0.4 nm depth interval and a reduction of the valley number in the $>$ 0.5 nm depth range. At this dose of implantation, the maximum valley depth is 3.5 nm and the maximum valley number is 432 at a depth of 0.3 nm.

AFM generally has different spatial resolution in different directions, with a high resolution along the vertical axis (down to 0.05 nm) but relatively poor resolution for the x- and y-axes. Therefore, it is difficult to directly observe and measure

Table I Roughness Analysis of the 6FDA-pMDA Samples

Sample	Mean Roughness (nm)	Peak Count (Height Threshold: 0.2 nm)	Peak Count (Height Threshold: 0.4 nm)	Peak Count (Height Threshold: 0.5 nm)
Nonimplanted sample	0.578	65	63	61
$2 \times 10^{14}/cm^2$	0.366	115	112	80
$1 \times 10^{15}/cm^2$	0.266	717	706	581
$5 \times 10^{15}/cm^2$	0.134	535	107	34

Table II Peak Count in Different Height Levels

Sample	Peak Count (0.2–0.4 nm)	Peak Count (0.4–0.5 nm)	Peak Count (>0.5 nm)
Nonimplanted sample	2	2	61
$2 \times 10^{14}/cm^2$	3	32	80
$1 \times 10^{15}/cm^2$	11	125	581
$5 \times 10^{15}/cm^2$	428	73	34

the micropore size of a gas separation membrane using conventional AFM. However, surface valley count in roughness analysis, which is based on the high vertical resolution, could provide an ideal tool to reveal information about the microvoid size and microvoid size distribution. It can be observed from the above AFM images that higher peaks are often related to deeper and larger valleys. The dramatic change in surface morphology of the films induced by ion implantation may explain the ion-irradiation effects on iodine diffusion and gas permeation properties in the polyimide films. Iodine atom may easily diffuse into the depths of the polyimide films through these deep valleys which exist in nonimplanted films. According to the theoretical calculation, the thickness of ion-beam-modified layer was about 490 nm. Ion bombardment of polymers causes scissions of chemical bonds, formation of free radicals, gas emission, crosslinking, and even—at high dose of irradiation—formation of new materials in the energy deposition range of the polymer films.[30] Therefore, ion-beam irradiation gives rise to a rearrangement of atoms in the film, alters microstructure of the surface layer, and forms a modified layer,

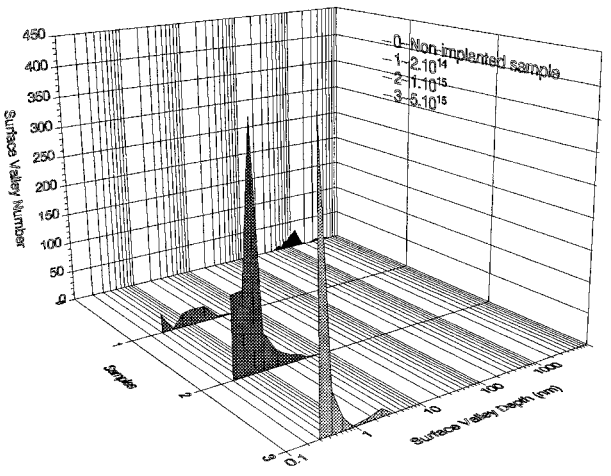

Figure 8 Distribution of surface valley number as function of depth for all of the implanted samples and the reference sample.

all of which eliminate the initial deep valleys and may significantly reduce further iodine diffusion into the depth of the film. The increase in the valley number of the small-dose sample relative to the reference material implies that the implantation introduced a great number of microvoids at the surface of the sample. Consequently, the small-dose-modified layer may play a double role in the observed iodine diffusion: on one hand, providing much more space for iodine diffusion in the layer due to a great number of microvoids induced by ion irradiation; on the other hand, reducing iodine diffusion beyond the modified layer by eliminating deep valleys. This also explains the very large increase in permeability of both H_2 and CH_4 with a corresponding decrease in selectivity for small-dose implantation.[16–18]

The small number of valleys on the scale of $>$ 0.5 nm, combined with the large number of valleys on a small scale (0.2–0.4 nm), imply that the high-fluence implantation induced a large number of small microvoids which may significantly slow the diffusion of iodine atoms and significantly reduce penetration of iodine into the film. A large number of small microvoids in the surface microstructure favors permeation of small molecules like H_2 while presenting resistance to the flux of large molecules such as CH_4. This agrees well with the simultaneous increase in H_2 permeability and H_2/CH_4 permselectivity following high-dose irradiation.[16–18] The modification of microstructure of the polymer induced by ion bombardment not only explains the previous results of iodine diffusion and gas permeation but may also find application to microelectronic packaging by providing a good adhesion between metallic connecting layers and polymeric dielectric layers while preventing potential diffusion of metallic species to improve reliability. Further study of ion beam-irradiation-induced changes in microvoid size and size distribution combined with the effect on gas transport properties are underway.

Figure 9 is a large-scale (100×100 μm in x, y-plane) top-view AFM image of the sample im-

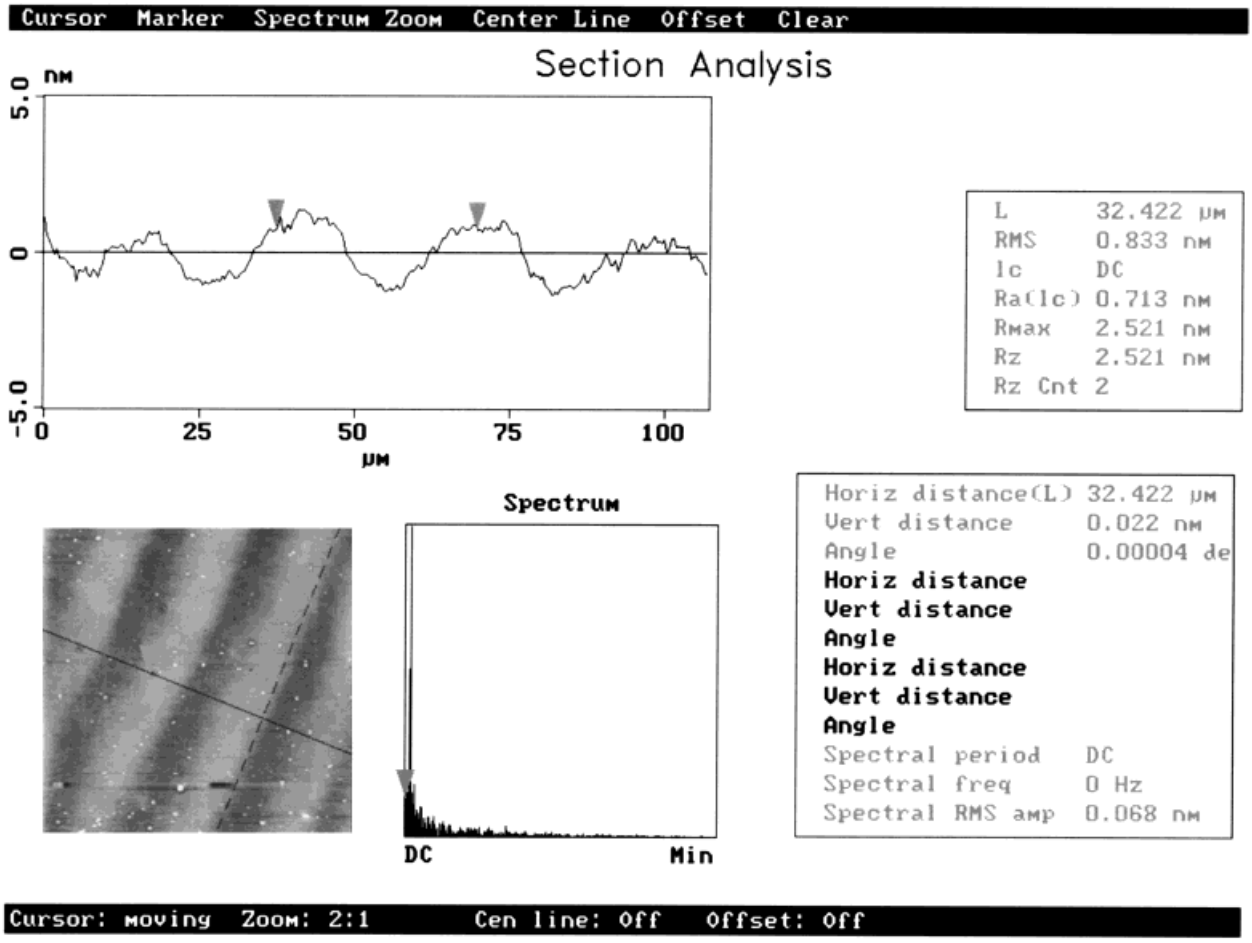

Figure 9 A section analysis plot of the high-fluence implanted 6FDA-pMDA polyimide sample. An ion beam-induced ripple topography with a wavelength of 25 μm can be observed.

planted with 5×10^{15} N^+/cm^2. A ripple topography with a wavelength of 25 μm can be observed. A detailed section analysis shows that the height between the high peak and valley bottom is about 2 nm. Ripple topographies[31–35] have been observed for amorphous solids such as glass, Araldite, fused silica, and vitreous carbon, and for crystalline solids such as copper, iron, and sapphire. The wavelength of this ripple is typically on the order of 0.1–1 μm. Ripple topography induced by ion-beam irradiation of polymers has not been reported. Further investigation is required to understand the mechanism of formation of the ripple structure in the irradiated sample.

CONCLUSIONS

AFM was used to investigate the topographical and morphological modification of 6FDA-pMDA polyimide films resulting from ion-beam irradiation. The freestanding polyimide films have deep valleys which can extend to a depth of several micrometers. Ion irradiation, even at a small dose, alters the microstructure of the surface and forms a modified layer with shallow valleys while eliminating the initial deep valleys. In addition, small-dose irradiation gives rise to many microvoids at the surface while the high-fluence irradiation induces the formation of many small microvoids in the surface. Observation of 3-D AFM images, along with detailed roughness and bearing analyses of these images, support the conclusions of our previous work on ion-beam irradiation effects on iodine diffusion and gas permeation of polyimide films. High-dose irradiation also induced in the surface a ripple topography with a wavelength of 25 μm and an amplitude of 2 nm.

The support of the National Science Foundation

through the Presidential Faculty Fellows Program (CTS-9553267) in funding this project is gratefully acknowledged. The authors thank Kevin Williams for the synthesis of the polyimide and Zixin Lin for the ion implantation. The authors gratefully acknowledge Professor Richard Ulrich for his help with the atomic force microscope, and the High Density Electronic Center at the University of Arkansas for the use of the equipment.

REFERENCES

1. K. Holloway, L. P. Buchwalter, and R. H. Lacombe, *J. Adhesion Sci. Technol.,* **7,** 1293 (1993).
2. J. M. Cech, A. F. Burnett, and C.-P. Chien, *IEEE Transactions on Components, Hybrids and Manufacturing Technology,* **16,** 752 (1993).
3. T. Miyagi, K. Itoh, S. Kimijima, and T. Sudo, *IEEE Transactions on Components, Hybrids and Manufacturing Technology,* **13,** 828 (1990).
4. G. M. Adema, I. Turlik, P. L. Smith, and M. J. Berry, *Proc. Electronic Components Conference,* Vol. 1, IEEE, Piscataway, NJ, 1990, p. 717.
5. S. F. Hubbard, K. D. Singer, F. Li, S. Z. D. Cheng, and F. W. Harris, *Appl. Phys. Lett.,* **65,** 265 (1994).
6. K. Y. Wong and A. K.-Y. Jen, *J. Appl. Phys.,* **75,** 3308 (1994).
7. M. R. Coleman, R. Kohn, and W. J. Koros, *J. Appl. Polym. Sci.,* **50,** 1059 (1993).
8. M. R. Coleman and W. J. Koros, *J. Membrane Sci.,* **50,** 285 (1990).
9. T.-H. Kim, W. J. Koros, and G. R. Husk, *J. Membrane Sci.,* **46,** 43 (1989).
10. L. M. Costello, W. J. Koros, *J. Polym. Sci., Part B: Polymer Phys. Ed.,* **33,** 135 146 (1995).
11. J. O. Borland, *Mat. Res. Soc. Symp. Proc.,* **354,** 123 (1995).
12. J.-P. Colinge, *Microelectronic Eng.,* **28,** 423 (1995).
13. J. Davenas, G. Boiteux, X. L. Xu, and E. Adem, *Nuclear Instruments & Methods in Physics Research, Section B: Beam Interactions with Materials and Atoms,* **B32,** 136 (1988).
14. G. Marletta, S. Pignataro, and C. Oliveri, *Nuclear Instruments & Methods in Physics Research, Section B: Beam Interactions with Materials and Atoms,* **B39,** 792 (1989).
15. D. Xu, X. L. Xu, and S. Zou, *Appl. Phys. Lett.,* **59,** 3110 (1991).
16. J. Davenas, X. L. Xu, *Nucl. Instr. and Methods,* **B71,** 33–38 (1992).
17. X. L. Xu, J. Y. Dolveck, G. Boiteux, M. Escoubes, M. Monchanin, J. P. Dupin, and J. Davenas, *Mat. Res. Soc. Symp. Proc.,* **354,** 351 (1995).
18. X. L. Xu, J. Y. Dolveck, G. Boiteux, M. Escoubes, M. Monchanin, J. P. Dupin, and J. Davenas, *J. Appl. Polym. Sci.,* **55,** 99 (1995).
19. S. A. Sundet, *J. Membrane Sci.,* **76**(2/3), 175 (1993).
20. G. Binnig, C. F. Quate, and Ch. Gerber, *Phys. Rev. Lett.,* **56,** 930 (1986); G. Binnig, Ch. Gerber, E. Stoll, T. R. Albrecht, and C. F. Quate, *Europhys. Lett.,* **3,** 1281 (1987).
21. O. Marti, B. Drake, and P. K. Hansma, *Appl. Phys. Lett.,* **51,** 484 (1987).
22. D. Rugar and P. Hansma, *Phys. Today,* **Oct.,** 23 (1990).
23. V. T. Vladimir and D. H. Reneker, *Macromolecules,* **28,** 1370 (1995).
24. A. K. Fritzsche, A. R. Arevalo, M. D. Moore, C. J. Weber, V. B. Elings, K. Kjoller, and C. M. Wu, *J. Appl. Polym. Sci.,* **46,** 167 (1992).
25. A. K. Fritzsche, A. R. Arevalo, M. D. Moore, and C. O'Hara, *J. Membrane Sci.,* **81,** 109 (1993).
26. A. K. Fritzsche, A. R. Arevalo, M. D. Moore, V. B. Elings, K. Kjoller, and C. M. Wu, *J. Membrane Sci.,* **68,** 65 (1992).
27. G. R. Husk, P. E. Cassidy, and K. L. Gebert, *Macromolecules,* **21,** 1234 (1988).
28. J. F. Ziegler, J. P. Biersack, and U. Littmark, in *The Stopping and Range of Ions in Solids,* Vol. 1, J. F. Ziegler, Ed., Pergamon Press, New York, 1985.
29. Command Reference Manual of NanoScope® III Scanning Probe Microscope Version 4.10, Digital Instruments, Santa Barbara, CA, USA, 1995.
30. X. L. Xu, These D'État ès Science, No. d'order 8708, Université Claude-Bernard-Lyon-I 1987.
31. R. S. Dhariwal and R. K. Fitch, *J. Mat. Sci.,* **12,** 1225 (1977).
32. M. Navez, C. Sella, and D. Chaperot, *C. R. Acad. Sci.,* **254,** 240 (1962).
33. T. Motohiro and Y. Taga, *Thin Solid Films,* **147,** 153 (1987).
34. G. W. Lewis, M. J. Nobes, G. Carter, and J. L. Whitton, *Nucl. Instrum. Meth.,* **170,** 363 (1980).
35. J. J. P. Elich, H. E. Roosendaal, H. H. Kersten, D. Onderdelinden, J. Kistemaker, and J. D. Elen, *Rad. Eff.,* **8,** 1 (1971).